

1 **The Entropic Braiding Index (*eBI*): a robust metric to account for the diversity of channel scales in**
2 **multi-thread rivers**

3 Alejandro Tejedor^{1,2*}, Jon Schwenk³, Maarten Kleinhans⁴, Ajay B. Limaye⁵, Lawrence Vulis², Paul
4 Carling⁶, Holger Kantz⁷, Efi Foufoula-Georgiou^{2,8}

5

6 ¹ Department of Science and Engineering, Sorbonne University Abu Dhabi, United Arab Emirates

7 ² Department of Civil and Environmental Engineering, University of California, Irvine, Irvine, California, USA

8 ³ Los Alamos National Laboratory, Division of Earth and Environmental Sciences, Los Alamos, NM, USA

9 ⁴ Faculty of Geosciences, Utrecht University, Utrecht, The Netherlands

10 ⁵ Department of Environmental Sciences, University of Virginia, Charlottesville, VA, USA

11 ⁶ Geography and Environmental Science, University of Southampton, Southampton, UK

12 ⁷ Max Planck Institute for the Physics of Complex Systems, Dresden, Germany

13 ⁸ Department of Earth System Science, University of California, Irvine, Irvine, California, USA

14 *Correspondence to: alejtejedor@gmail.com

15

16

17

18

19

20

21

22

23 **Abstract**

24 The Braiding Index (BI), defined as the average count of intercepted channels per cross-section, is a
 25 widely used metric for characterizing multi-thread river systems. However, it does not account for the
 26 diversity of channels (e.g., in terms of discharge) within different cross-sections, omitting important
 27 information related to system complexity. Here we present a modification of BI (the Entropic Braiding
 28 Index, eBI) which augments the information content in BI by using Shannon Entropy to encode the
 29 diversity of channels in each cross section. eBI is interpreted as the number of “effective channels” per
 30 cross-section, allowing a direct comparison with the traditional BI . We demonstrate the superior
 31 capabilities of eBI via analysis of synthetic, numerical and field examples. In addition, we show that
 32 interrogating cross-sections via the ratio BI/eBI has the potential to quantify channel disparity,
 33 differentiate types of multi-thread systems, and inform about cross-section stability to forcing variability
 34 (e.g., seasonal flooding).

35

36

37

38

39

40

41

42

43

44

45 **1. Introduction**

46 Channels routing water and sediment across the Earth’s surface exhibit different configurations, ranging
 47 from single-thread (straight and meandering) to multi-thread (braided, anabranching and anastomosing)
 48 patterns (Eaton et al., 2010; Huang & Nanson, 2007; Leopold & Wolman, 1957). Our ever-increasing
 49 capacity to observe Earth’s surface via remote sensing allows us not only to characterize these patterns
 50 globally but also witness their dynamic nature by using the archive of nearly 50 years of satellite imagery
 51 (e.g., Landsat).

52 Braided rivers exhibit intricate and complex patterns while being highly dynamic, wherein their channel-
 53 bar complex can be substantially reconfigured including due to seasonal flooding. Although significant
 54 strides have been made to better characterize and understand the multi-scale dynamics of these complex
 55 systems, e.g. using space-time renormalization theory (e.g., Foufoula-Georgiou & Sapozhnikov, 2001;
 56 Sapozhnikov et al., 1998; Sapozhnikov & Foufoula-Georgiou, 1999) or network theory (e.g., Marra et al.,
 57 2014), the most commonly adopted indices to quantify the *braiding intensity* of a river (Egozi &
 58 Ashmore, 2008) focus on bar properties, channel count, or channel sinuosity. Particularly, as the defining
 59 characteristic of a braided river is its multiple channel threads, the most commonly applied metric of a
 60 braided river—the braiding index *BI*—captures this essential characteristic by counting the number of
 61 channel threads per river cross-section (e.g., Egozi & Ashmore, 2009; Fischer et al., 2015; Kleinhans &
 62 van den Berg, 2011; Limaye, 2017; Limaye et al., 2018; Meshkova & Carling, 2013; Nicholas, 2013).
 63 However, despite its wide use, this index has important limitations: (1) *It is a simple count* – and is
 64 therefore insensitive to the differences in discharge and sediment flux between adjacent threads, which
 65 can vary by orders of magnitude (see Figure 1b for an example of channel heterogeneity in a cross-
 66 section). (2) *It is sensitive to resolution* – as the resolution is increased, smaller channels can be observed,
 67 varying the value of *BI* abruptly. This resolution dependence is problematic because advances in satellite
 68 imaging in recent years have created an historical archive of data that spans a wide range in resolution. (3)
 69 *It is sensitive to water level* – the channel count is highly sensitive to flow discharge and stage,

70 increasing the number of flooded channels in intermediate discharge but decreasing the number in
71 extreme floods that submerges the bars. These limitations in this characteristic metric of braided rivers
72 hinder our ability to understand the complexity of these systems relative to the underlying relevant
73 physical variables, as well as to compare geometry across systems (Carling et al., 2014).

74 Here, we propose a new metric for braiding intensity called the Entropic Braiding Index, *eBI*, which
75 addresses the crucial limitations noted above for *BI*. The *eBI* is more robust to changes in resolution and
76 acknowledges the discharge heterogeneity of the channels co-existing in a given cross-section, while
77 keeping some of the key properties of the traditional *BI*, i.e., its simplicity, interpretability, and relevance
78 to the essential multithread nature of braided rivers. As we demonstrate in this work, *eBI* can be
79 interpreted as the *effective number of channels* per cross-section. The definition of effective number of
80 channels is rooted in a probabilistic Lagrangian view of transport, the uncertainty of which is
81 characterized by Shannon Entropy (Shannon, 1948), resulting in a metric that suitably integrates the
82 information of the channel count and the relative size of the channels (e.g., in terms of discharge) per
83 cross-section.

84 In what follows, we first briefly introduce the concept of Shannon Entropy as a measure of uncertainty,
85 which is the basis for defining the *eBI*. We continue with a comparison of *BI* and *eBI* through some
86 illustrative examples, application to the characterization of a field case, and finally different numerically
87 simulated braided rivers with varying sediment size and with and without vegetation. We conclude with a
88 discussion of the potential of this new index to not only characterize multi-thread systems more robustly
89 but also to indicate system stability.

90

91 **2. Shannon Entropy**

92 The cornerstone of information theory is Shannon Entropy, which quantifies the uncertainty in the
93 outcome of a stochastic process (e.g., flipping a coin or rolling a die). In other words, Shannon Entropy

94 quantifies the amount of information needed to describe (on average) the resulting outcome of a
 95 stochastic process (Cover & Thomas, 2006). Uncertainty can be derived intuitively from the notions of
 96 probability and surprise. For a given discrete stochastic process $\{x_i\}$, such as rolling a die, with a
 97 specified probability distribution of outcomes, for example $\{p_1 = 5/6; , p_2 = 1/6\}$ for a six-sided die
 98 with five sides numbered with one and one side numbered with two. Intuitively, the occurrence of rolling
 99 a one is less surprising than rolling a two. Mathematically, the surprise associated with a given outcome x_i
 100 can be expressed as $-\log(p_i)$, which matches our intuitive notion of surprise: the occurrence of outcome
 101 with probability one, $p_i = 1$ (e.g., rolling a number smaller than three in the die described above),
 102 produces zero surprise since $-\log(1) = 0$; while the occurrence of an impossible outcome, $p_i = 0$ (e.g.
 103 rolling a three with the die described above), would produce an infinite surprise since $-\log(0) = \infty$.
 104 The uncertainty of a particular outcome, h_i , is defined as the surprise that this outcome produces,
 105 $-\log(p_i)$, times the probability of its occurrence p_i . Therefore, the uncertainty associated with either a
 106 completely certain event ($p_i = 1$) or an impossible one ($p_i = 0$) is zero. The uncertainty, or Shannon
 107 Entropy H , associated with a discrete stochastic process, with N possible outcomes with probabilities
 108 $\{p_1, p_2, \dots, p_i, \dots, p_N\}$, is equal to the sum of the uncertainties introduced by each outcome x_i :

109
$$H = \sum_{i=1}^N h_i = - \sum_{i=1}^N p_i \log_2 p_i \quad (1)$$

110 Note that traditionally the logarithm used is in base 2, which is reminiscent of the origin of Shannon
 111 Entropy within the field of signal processing, where the \log_2 leads to the interpretation of its value in
 112 terms of bits of information. A different interpretation of the value of H , when computed using the \log_2 , is
 113 the minimum number of yes/no questions that are needed to determine, on average, the outcome of the
 114 stochastic process.

115 H is maximal ($H_{\max}(N)$) when all the N possible outcomes have the same probability of occurrence $1/N$,
 116 for example rolling a fair six-faced die with a different number on each face and each having a probability

117 of occurrence $1/6$ (Cover & Thomas, 2006). Note that $H_{\max}(N)$ scales logarithmically with the number of
 118 possible outcomes N .

119
$$H_{\max}(N) = \sum_{i=1}^N h_i = - \sum_{i=1}^N \frac{1}{N} \log_2 \frac{1}{N} = -N \left(\frac{1}{N} \log_2 \frac{1}{N} \right) = \log_2 N \quad (2)$$

120

121 **3. Defining the entropic braiding index, eBI**

122 In this section we utilize a series of examples to illustrate the applicability of Shannon entropy to
 123 characterize multi-thread rivers, introducing the concept of the entropic braiding index, eBI , and pointing
 124 out some of the advantages of the new metric when compared with the traditional BI . Particularly, Fig 1a
 125 shows a synthetic example of six river cross-sections, each of them containing four channel threads, and
 126 therefore characterized by $BI = 4$. This example highlights the fact that the characterization of a multi-
 127 thread river via BI is quite coarse because the simple channel count ignores the relative size of the co-
 128 existing channels (e.g., in terms of discharge) at the cross-section.

129 We propose using Shannon entropy as a more robust and meaningful characterization of the cross-
 130 sectional properties of multi-thread rivers. In this case, the problem may be reformulated from the point of
 131 view of probabilistic Lagrangian transport. A tracer injected upstream of the multi-thread channel has a
 132 certain probability to eventually go through each of the different channel threads at a given cross-section.
 133 Each cross-section of the full river can be abstracted as a stochastic process with a number of outcomes
 134 equal to the number of channel threads observed at that cross-section (i.e., four for all the cases shown in
 135 Fig 1a), and each outcome with probability given by the relative flow of the corresponding channel thread
 136 with respect to the total flow conveyed by all channels at that cross-section. Thus, the Shannon entropy
 137 associated to each cross-section, H , can be computed as follows

138
$$H = \sum_{i=1}^N h_i = - \sum_{i=1}^N \frac{q_i}{Q} \log_2 \frac{q_i}{Q} \quad (3)$$

139 where q_i is the flow going through channel i in that cross-section, and $Q = \sum q_i$ is the total discharge
 140 going through that cross-section (Fig 1a shows the ratio $\frac{q_i}{Q}$, which can be interpreted as probability, to the
 141 left of each band). The value of H is the highest (given a channel count) for systems consisting of
 142 channel threads carrying equal flow (i.e., leftmost column in Fig 1a) because this case maximizes the
 143 uncertainty for the path of a tracer particle. In contrast, systems dominated by a single channel are
 144 characterized by low values of H due to low path uncertainty (i.e., rightmost column in Fig 1a). Figure 1c
 145 also shows the robustness of this metric under different resolutions. In particular, Fig 1c presents a
 146 synthetic scenario wherein, by increasing the resolution, an apparently singular channel thread in Fig 1a is
 147 resolved as two different channels at the finer resolution (the example uses the two endmembers from Fig
 148 1a – the left- and rightmost columns – where the top channel is resolved as two different channels in Fig
 149 1c under higher resolution). While the traditional BI jumps from 4 to 5 under the increasing resolution
 150 scenario, the change in the value of H (from 2 to 2.06) reflects more suitably the addition of a very narrow
 151 channel with minimal flow.

152 Although H is a suitable metric to directly characterize multi-thread systems, unlike the traditional
 153 braiding index, its value is not directly interpretable in terms of a geomorphic feature. More importantly,
 154 it is not straightforward to compare H with more widely used metrics such as BI . To overcome these
 155 issues, we propose to define the entropic Braiding Index, eBI , as

$$156 \quad eBI = 2^H \quad (4)$$

157 eBI is an increasing function of H , and according to equation 2, can be interpreted as the equivalent
 158 number of channels that a multi-thread system consisting of identical (in terms of discharge) channels
 159 would have. Thus, eBI is interpreted here as an *effective channel count* that integrates the information
 160 relative to the number of channels together with the relative importance of those channels in terms of
 161 discharge. Note that for a system where all the channels exhibit equal discharge, i.e., $q_i = Q/N \forall i$, then
 162 eBI achieves the same value as the traditional BI . As shown in Fig 1, eBI captures important information
 163 elusive to BI , while offering an interpretable value that intuitively reflects the number of effective

164 channels occur per cross-section. Finally, Figure 1c shows that, under an increase in resolution, eBI is
 165 much more robust than the traditional BI .

166

167 **4. eBI in action**

168 In the first part of this section, we present a field case comparison of the traditional BI and the new eBI .

169 We further discuss the properties of eBI by characterizing the braiding intensity of different multi-thread

170 rivers in numerical simulations, where several variables such as water discharge, vegetation, or sediment

171 size were controlled. Channel width has been argued to be a good proxy for estimating water discharge in

172 braided systems (Ashmore, 2007; Fahnestock, 1963; Gaurav et al., 2015). Note that for consistency and

173 simplicity in our analysis, we have used channel width as a proxy for the water discharge partition both

174 for the field case and the numerically simulated systems, but the framework is applicable for any system-

175 specific nonlinear function of discharge and width. Thus, the definition of the Shannon entropy for each

176 cross-section is

177
$$H = \sum_{i=1}^N h_i = - \sum_{i=1}^N \frac{w_i}{W} \log_2 \frac{w_i}{W} \quad (6)$$

178 where for each cross-section: N is the number of channels, w_i is the width of its i^{th} channel, and $W =$

179 $\sum_{i=1}^N w_i$ is the total wet width (note the ratio $\frac{w_i}{W}$ can be interpreted as a probability). Using this definition

180 of H , eBI is computed as 2^H .

181

182 *4.1. Insight from the Indus River*

183 We analyzed a braided section of the Indus River at mean annual discharge. We used a 30-m spatial

184 resolution mask from the Global River Widths from Landsat database (Allen & Pavelsky, 2018) with the

185 Python package *RivGraph* (Schwenk et al., 2020; Schwenk & Hariharan, 2021) to automatically obtain
186 channel counts and widths, generate transects, and compute BI and eBI across each transect.

187 Figure 2a shows the locations of several cross sections whose corresponding measurements of braiding
188 intensity are shown in Figure 2b. This comparison showcases the key properties of eBI with regard to the
189 traditional BI : (1) *eBI is more informative and robust* – eBI provides information about the changes in the
190 planform geometry of the multi-thread system in terms of distribution of discharge among the active
191 channels, while BI is insensitive to these properties. For example, Fig 2c shows a transect at which the
192 traditional BI is more than double the eBI due to the presence of very small channels (relative to the
193 widest one). At the same time, eBI is more robust to changes in resolution, as illustrated with the
194 schematic in Fig 1c. (2) *BI is an upper bound for eBI* – We note that by definition, eBI is equal to BI
195 when all the channels co-existing in a given cross-section have equal probability of receiving fluxes from
196 upstream (i.e., in this analysis in terms of width). Any other configuration results in a value of eBI lower
197 than BI . Moreover, note that it is possible that two cross-sections with a different BI could be
198 characterized by the same (or very similar) number of effective channels as defined by eBI . (3) *BI/eBI*
199 *quantifies channel heterogeneity* – From the mathematical point of view, the value of eBI accounts both
200 for the number of channels and their relative size (in terms of discharge or width), while BI solely
201 accounts for the channel count. Consequently, BI/eBI (red curve in Fig 2b), far from being random, i.e., BI
202 and eBI are not completely independent variables, is key in the characterization of the system, because it
203 is related to the heterogeneity in the channels present in the different cross-sections (the more variable the
204 channels are in terms of width, the higher the ratio of the two indices).

205 The eBI features discussed above significantly improve the characterization of multi-thread systems in
206 contrast to BI as they provide additional valuable information about the whole system, while being simple
207 to compute from local (cross-sectional) information only, as opposed to other whole-network metrics
208 based on graph theory (e.g., Marra et al., 2014; Tejedor et al., 2015a, 2015b, 2016, 2017, 2018).

209 Furthermore, some interesting questions emerge from the comparison between BI and eBI , and
 210 particularly from the ratio BI/eBI . For example: (1) how different are these two indices at different levels
 211 of discharge, or for different types of multi-thread systems? (2) Does this difference shed light on the
 212 dynamics of the cross-sections? Or in other words, are cross-sections characterized by a large value of
 213 BI/eBI (heterogeneous cross-section in terms of channel thread discharge) more prone to be reconfigured
 214 by flooding? We utilized numerical simulations as a preliminary analysis on these questions.

215

216 *4.2. Using eBI for insight into multi-thread river types and dynamics*

217 In the interest of characterizing systems under different hydrologic conditions but in a controlled
 218 environment and for long time spans, we present here the results corresponding to the analysis of different
 219 multi-thread systems obtained from numerical simulations. Particularly, we utilized some of the model
 220 outputs presented by Kleinhans et al., (2018) for the River Allier (France), which were obtained using the
 221 depth-averaged version of Delft3D, with the vegetation module developed by (van Oorschot et al., (2017)).
 222 Sediment transport was modeled in the same manner as in Braat et al., (2017). From all the runs
 223 presented in Kleinhans et al., (2018), we chose five runs (see Fig 3b for a table containing the key
 224 parameters) that offered a broad range of variability from the geomorphologic point of view, ranging from
 225 an anastomosing system with more stable banks to very active braided systems.

226 Each of the numerical experiments analyzed in this section was set up with the boundary conditions
 227 corresponding to the River Allier and were initialized with a set of symmetrical bends (for more details
 228 see (Kleinhans et al., 2018)). For each run, the system was forced by a 300-year (except for Run 5 with a
 229 150-year) time series of discharge between 50 and 400 m^3s^{-1} , randomly sampled from five typical flood
 230 hydrographs.

231 For each run, we extracted two water masks (low and high flow) per year of the simulation by simply
 232 thresholding on water depth. Each of those water masks was analyzed using RivGraph to obtain the

233 channel count and channel widths per cross-section (here as in the case of observational data, we use
234 channel width as a proxy for discharge for consistency). In our analysis, we discarded the first 75 years
235 for each simulation to avoid the effects of initial conditions. For similar reasons, 30% of the spatial
236 domain (15% from the upstream and 15% from the downstream boundaries) was discarded to avoid
237 spurious effects introduced by the upstream and downstream boundary conditions.

238 For each run, multi-thread patterns of different complexity and degree of dynamism emerged (See Fig 3a
239 for an instance of one of the simulations for illustration purposes). The analysis of these systems
240 according to the *eBI*, as well as its comparison with the traditional *BI*, yields the following important
241 remarks as revealed within Fig 3c: (1) *Regarding low vs. high flow conditions*: As expected, the *eBI* for
242 low flow conditions is significantly lower than for those corresponding to high flow conditions. This
243 expected result is also reflected in the analysis of the system via the *BI*, which documents the activation of
244 fewer channels during the low flow conditions when compared with the higher discharge. However, some
245 key information is revealed by the *eBI* when compared with *BI* - channels co-existing in the different
246 cross-sections at the low discharge regime are more uniform in terms of widths as captured by the small
247 value of *BI/eBI*, while at higher discharge levels the width disparity among channels increases as a
248 consequence of the activation of small channels, which can be an order of magnitude smaller than the
249 dominant channels conveying most of the water and sediment. (2) *Braided vs Anastomosing systems*:
250 From all the model runs analyzed, run 5 corresponds to an anastomosing system, while the other four runs
251 could be classified as braided systems. From our analysis, we can conclude that the anastomosing system
252 develops channels less diverse in width compared with braided river systems even at high flow regimes,
253 as is evident from the significantly smaller values of *BI/eBI* for the anastomosing system (run 5), in
254 comparison with the braided rivers (runs 1-4).

255 Given the interest in identifying possible emergent behavior of these complex systems in
256 response to perturbations or future forcing, we posed the following question: does channel heterogeneity
257 provide information about the potential (in)stability in terms of maintaining the number of threads of a

258 specific cross section? Or, in other words, are cross-sections characterized by a higher channel-width
 259 disparity less stable to perturbations than those cross-sections of more uniform channels in terms of
 260 widths? To shed light on this question, we performed the following analysis. For each model run, we
 261 monitored the temporal evolution of each cross-section, in which we discretized the spatial domain (74
 262 cross-sections). Specifically, we analyzed the system evolution retrospectively, documenting every time
 263 that a cross-section was reconfigured in terms of experiencing a change in its number of co-existing
 264 channels. For those reconfigurations, we recorded the time, the cross-section location, the new number of
 265 co-existing channels, and their persistence, i.e., the number of years (in model time) for which the new
 266 number of channels was sustained in that cross-section. Thus, we define a “*k*-year, *n*-channel stable cross-
 267 section” as a cross-section that was able to maintain *n*-channels for a period of *k* years or more. Given
 268 this definition, the question that we want to address is whether *k*-year, *n*-channel stable cross-sections are
 269 characterized by a different degree of channel similarity (in terms of width) than that corresponding to *k*-
 270 year *n*-channel *unstable* cross-sections. In other words, are systems with less diverse channels exhibiting
 271 more or less stability (persistence) in maintaining those channels over long time periods? Note that
 272 because in our analysis we were controlling the number of channels per cross-section, *n*, channel
 273 similarity is directly quantified by the number of effective channels, *eBI* (the more homogeneous are the
 274 channels in terms of width the closer the number of effective channels is to *n*). Given the spatiotemporal
 275 domain offered by the model runs as well as the characteristics of the model parameters, we present our
 276 analysis only for *k*-year 2-channel (un-)stable cross-sections (for *k*=5,10,15 and 20 years) as for *n*>2 the
 277 number of occurrences is too limited to show statistically robust results. Particularly, for each model run
 278 and threshold of temporal stability (*k*=5,10, 15 and 20 years), we computed the difference, Δ , between the
 279 mean *eBI* for unstable and stable cross-sections:

$$280 \quad \Delta = \langle eBI \rangle_{k\text{-year}, 2\text{-channel stable cross-section}} - \langle eBI \rangle_{k\text{-year}, 2\text{-channel unstable cross-section}} \quad (7)$$

281 where a system characterized by $\Delta > 0$ exhibits stable cross-sections with a higher number of effective
 282 channels, i.e., stable cross-sections are on average more homogeneous in terms of channel widths; while

283 $\Delta < 0$ corresponds to systems for which stable cross-sections on average exhibit a higher channel width
 284 disparity (heterogeneous cross-sections), and therefore, smaller eBI .

285 The results of our analysis (see Fig 3d) show three different scenarios: (a) *Runs 1, 2, and 3*: Stable cross-
 286 sections are characterized by more uniform channels than unstable cross-sections. The three runs showing
 287 this behavior have in common different mechanisms of channel stability (sediment cohesion and/or
 288 vegetation). In those cases, co-existing channels of similar size are able to create channel structures in the
 289 floodplain that are more stable given variations in discharge, while co-existing relatively smaller channels
 290 are less likely to generate positive feedbacks with vegetation and/or establish stable banks (cohesive
 291 sediment) maintaining their structure and geometry during more extended periods of time. (b) *Run 4 –*
 292 *Only Sand*: Cross-section stability is characterized by a larger channel disparity in comparison with the
 293 unstable counterparts. The higher channel mobility in unstable systems allows the co-existence of
 294 channels of different sizes, although with large variability in the nature of the co-existing channels in
 295 terms of their relative discharge, as shown by negative values of Δ . (c) *Run 5 -Anastomosing system*: In
 296 this case, it appears that channel width disparity is not a good explanatory variable of cross-section
 297 stability, because both stable and unstable cross-sections yield values of Δ close to zero. We attribute this
 298 outcome to the fact that the channels present in anastomosing systems are consistently more uniform
 299 across the spatio-temporal domain of the run, as shown and discussed before (see Fig 2c) and therefore
 300 distinguishing between stable and unstable cross-sections might require a more detailed study.

301 Although the previous analysis is by no means a systematic analysis of cross-section channel stability, it
 302 nevertheless presents evidence of the potential of the new metric introduced here, eBI , to not only
 303 characterize the static patterns of multi-thread systems but also to serve as a tool for studying system
 304 response to forcing in terms of the dynamic behavior and stability of channels.

305

306

307 5. Conclusions and perspectives

308 Multi-thread fluvial systems are some of the most astonishing and intricate patterns observed on the
309 Earth's surface. Their complexity and dynamic nature hinder their characterization and our predictive
310 ability related to their evolution and response to future forcings. Many metrics have been proposed to
311 characterize those systems (e.g., channel count, channel link length, island geometry, etc.) but the
312 Braiding Index (*BI*) has been widely used as it is a simple measure of the number of channels intercepted
313 at a section, averaged over several cross sections of the system. By definition, *BI* does not account for
314 channel heterogeneity, *i.e.*, all channels are counted equally no matter how different they are in terms of
315 water discharge, width, etc., and precisely because of this, the *BI* is very sensitive to changes in the
316 resolution at which the system is analyzed; higher resolution images would reveal finer-scale channels
317 and thus higher *BI*. Despite these significant limitations, *BI* is widely used partly due to its simplicity in
318 computation and interpretation.

319 We propose a modification of the *BI* which accounts not only for the count but also for the heterogeneity
320 of channels in multi-thread river systems. We augmented the information content of each cross section
321 using an entropy metric that quantifies the diversity of channels (in terms of flow, channel width or any
322 other relevant property) in each cross section. We defined an entropic *BI* (*eBI*) and interpret it as the
323 number of effective channels per cross-section, allowing a direct comparison with the traditional *BI*, and
324 the gain of insightful information from the difference of the two indices.

325 We showed via analysis of synthetic examples and field and numerical cases that *eBI* contains much more
326 information about the system complexity than *BI*, being at the same time a more robust metric than *BI* as
327 incorporating significantly narrower channels (e.g., due to increasing observational resolution) does not
328 dramatically change *eBI* statistics. In addition, we proposed that interrogating cross-sections in terms of
329 the value BI/eBI has the potential to: (1) quantify channel disparity (e.g., in terms of width, discharge or
330 sediment transport capacity) per cross-section (ii) differentiate braided and anastomosing systems; and
331 (iii) provide information about cross-section stability to forcing (e.g., seasonal flooding).

332 **Acknowledgements**

333 E.F.G., L.V. and A.T. received partial support from NSF Grants EAR-1811909, DMS-1839336, and the
 334 UK Research and Innovation Global Challenges Research Fund Living Deltas Hub Grant NES008926.
 335 Moreover, L.Vulis was supported under the NASA Earth and Space Science Fellowship Program Grant
 336 0NSSC18K1409 and the UC-National Lab In-Residence Graduate Fellowship Grant L21GF3569. JS was
 337 supported by the Laboratory Directed Research and Development program of Los Alamos National
 338 Laboratory under project number 20170668PRD1.

339

340 **References**

341 Allen, G. H., & Pavelsky, T. M. (2018). Global extent of rivers and streams. *Science*, *361*(6402), 585–
 342 588. <https://doi.org/10.1126/science.aat0636>

343 Ashmore, P. E. (2007). Laboratory modelling of gravel braided stream morphology. *Earth Surface*
 344 *Processes and Landforms*, *7*(3), 201–225. <https://doi.org/10.1002/esp.3290070301>

345 Braat, L., Van Kessel, T., Leuven, J. R. F. W., & Kleinhans, M. G. (2017). Effects of mud supply on
 346 large-scale estuary morphology and development over centuries to millennia. *Earth Surface*
 347 *Dynamics*, *5*(4), 617–652. <https://doi.org/10.5194/esurf-5-617-2017>

348 Carling, P., Jansen, J., & Meshkova, L. (2014). Multichannel rivers: Their definition and classification.
 349 *Earth Surface Processes and Landforms*, *39*(1), 26–37. <https://doi.org/10.1002/esp.3419>

350 Cover, T. M., & Thomas, J. A. (2006). Elements of Information Theory. In *Elements of Information*
 351 *Theory* (2nd ed.). John Wiley and Sons Inc.

352 Eaton, B. C., Millar, R. G., & Davidson, S. (2010). Channel patterns: Braided, anabranching, and single-
 353 thread. *Geomorphology*, *120*(3–4), 353–364. <https://doi.org/10.1016/j.geomorph.2010.04.010>

354 Egozi, R., & Ashmore, P. (2008). Earth Surface Processes and Landforms Earth Surf. *Earth Surf.*
 355 *Process. Landforms*, *33*, 2121–2138. <https://doi.org/10.1002/esp>

356 Egozi, R., & Ashmore, P. (2009). Experimental analysis of braided channel pattern response to increased
 357 discharge. *Journal of Geophysical Research: Earth Surface*, *114*(2).
 358 <https://doi.org/10.1029/2008JF001099>

359 Fahnstock, R. K. (1963). Morphology and hydrology of a glacial stream -- White River, Mount Rainier,
 360 Washington. *Survey Professional Paper 422-A*. <https://doi.org/10.3133/pp422A>

361 Fischer, J., Kleidon, A., & Dittrich, P. (2015). Thermodynamics of random reaction networks. *PLoS*
 362 *ONE*, *10*(2). <https://doi.org/10.1371/journal.pone.0117312>

- 363 Foufoula-Georgiou, E., & Sapozhnikov, V. (2001). Scale Invariances in the Morphology and Evolution of
 364 Braided Rivers. *Mathematical Geology*, 33, 273–291.
 365 <https://doi.org/10.1023/A:1007682005786>
- 366 Gaurav, K., Métivier, F., Devauchelle, O., Sinha, R., Chauvet, H., Houssais, M., & Bouquerel, H. (2015).
 367 Morphology of the Kosi megafan channels. *Earth Surface Dynamics*, 3(3), 321–331.
 368 <https://doi.org/10.5194/esurf-3-321-2015>
- 369 Huang, H. Q., & Nanson, G. C. (2007). Why some alluvial rivers develop an anabranching pattern. *Water*
 370 *Resources Research*, 43(7). <https://doi.org/10.1029/2006WR005223>
- 371 Kleinans, M. G., de Vries, B., Braat, L., & van Oorschot, M. (2018). Living landscapes: Muddy and
 372 vegetated floodplain effects on fluvial pattern in an incised river. *Earth Surface Processes and*
 373 *Landforms*, 43(14), 2948–2963. <https://doi.org/10.1002/esp.4437>
- 374 Kleinans, M. G., & van den Berg, J. H. (2011). River channel and bar patterns explained and predicted
 375 by an empirical and a physics-based method. *Earth Surface Processes and Landforms*, 36(6), 721–
 376 738. <https://doi.org/10.1002/esp.2090>
- 377 Leopold, L. B., & Wolman, M. G. (1957). River channel patterns-braided, meandering and straight. *US*
 378 *Geological Survey Professional Paper*, 282B, 29–85.
- 379 Limaye, A. B. (2017). Extraction of Multithread Channel Networks With a Reduced-Complexity Flow
 380 Model. *Journal of Geophysical Research: Earth Surface*, 122(10), 1972–1990.
 381 <https://doi.org/10.1002/2016JF004175>
- 382 Limaye, A. B., Grimaud, J. L., Lai, S. Y. J., Foreman, B. Z., Komatsu, Y., & Paola, C. (2018). Geometry
 383 and dynamics of braided channels and bars under experimental density currents. *Sedimentology*,
 384 65(6), 1947–1972. <https://doi.org/10.1111/sed.12453>
- 385 Marra, W. A., Kleinans, M. G., & Addink, E. A. (2014). Network concepts to describe channel
 386 importance and change in multichannel systems: Test results for the Jamuna River, Bangladesh.
 387 *Earth Surface Processes and Landforms*, 39(6), 766–778. <https://doi.org/10.1002/esp.3482>
- 388 Meshkova, L. V., & Carling, P. A. (2013). Discrimination of alluvial and mixed bedrock-alluvial
 389 multichannel river networks. *Earth Surface Processes and Landforms*, 38(11), 1299–1316.
 390 <https://doi.org/10.1002/esp.3417>
- 391 Nicholas, A. (2013). Morphodynamic diversity of the world’s largest rivers. *Geology*, 41(4), 475–478.
 392 <https://doi.org/10.1130/G34016.1>
- 393 Sapozhnikov, V. B., & Foufoula-Georgiou, E. (1999). Horizontal and vertical self-organization of braided
 394 rivers toward a critical state. *Water Resources Research*, 35(3), 843–851.
 395 <https://doi.org/10.1029/98WR02744>
- 396 Sapozhnikov, V. B., Murray, A. B., Paola, C., & Foufoula-Georgiou, E. (1998). Validation of braided-
 397 stream models: Spatial state-space plots, self-affine scaling, and island shapes. *Water Resources*
 398 *Research*, 34(9), 2353–2364. <https://doi.org/10.1029/98WR01697>
- 399 Schwenk, J., & Hariharan, J. (2021). RivGraph: Automatic extraction and analysis of river and delta
 400 channel network topology. *Journal of Open Source Software*, 6(59), 2952.
 401 <https://doi.org/10.21105/joss.02952>

402 Schwenk, J., Piliouras, A., & Rowland, J. C. (2020). Determining flow directions in river channel
 403 networks using planform morphology and topology. *Earth Surface Dynamics*, 8(1), 87–102.
 404 <https://doi.org/10.5194/esurf-8-87-2020>

405 Shannon, C. E. (1948). A Mathematical Theory of Communication. *Bell System Technical Journal*, 27(4),
 406 623–656. <https://doi.org/10.1002/j.1538-7305.1948.tb00917.x>

407 Tejedor, A., Longjas, A., Caldwell, R., Edmonds, D. A., Zaliapin, I., & Foufoula-Georgiou, E. (2016).
 408 Quantifying the signature of sediment composition on the topologic and dynamic complexity of
 409 river delta channel networks and inferences toward delta classification. *Geophysical Research*
 410 *Letters*, 43(7). <https://doi.org/10.1002/2016GL068210>

411 Tejedor, A., Longjas, A., Edmonds, D. A., Zaliapin, I., Georgiou, T. T., Rinaldo, A., & Foufoula-
 412 Georgiou, E. (2017). Entropy and optimality in river deltas. *Proceedings of the National Academy of*
 413 *Sciences of the United States of America*, 114(44). <https://doi.org/10.1073/pnas.1708404114>

414 Tejedor, A., Longjas, A., Passalacqua, P., Moreno, Y., & Foufoula-Georgiou, E. (2018). Multiplex
 415 Networks: A Framework for Studying Multiprocess Multiscale Connectivity Via Coupled-Network
 416 Theory With an Application to River Deltas. *Geophysical Research Letters*, 45(18).
 417 <https://doi.org/10.1029/2018GL078355>

418 Tejedor, A., Longjas, A., Zaliapin, I., & Foufoula-Georgiou, E. (2015a). Delta channel networks: 1. A
 419 graph-theoretic approach for studying connectivity and steady state transport on deltaic surfaces.
 420 *Water Resources Research*, 51(6), 3998–4018. <https://doi.org/10.1002/2014WR016577>

421 Tejedor, A., Longjas, A., Zaliapin, I., & Foufoula-Georgiou, E. (2015b). Delta channel networks: 2.
 422 Metrics of topologic and dynamic complexity for delta comparison, physical inference, and
 423 vulnerability assessment. *Water Resources Research*, 51(6), 4019–4045.
 424 <https://doi.org/10.1002/2014WR016604>

425 van Oorschot, M., Kleinhans, M. G., Geerling, G. W., Egger, G., Leuven, R. S. E. W., & Middelkoop, H.
 426 (2017). Modeling invasive alien plant species in river systems: Interaction with native ecosystem
 427 engineers and effects on hydro-morphodynamic processes. *Water Resources Research*, 53(8), 6945–
 428 6969. <https://doi.org/10.1002/2017WR020854>

429

430

431

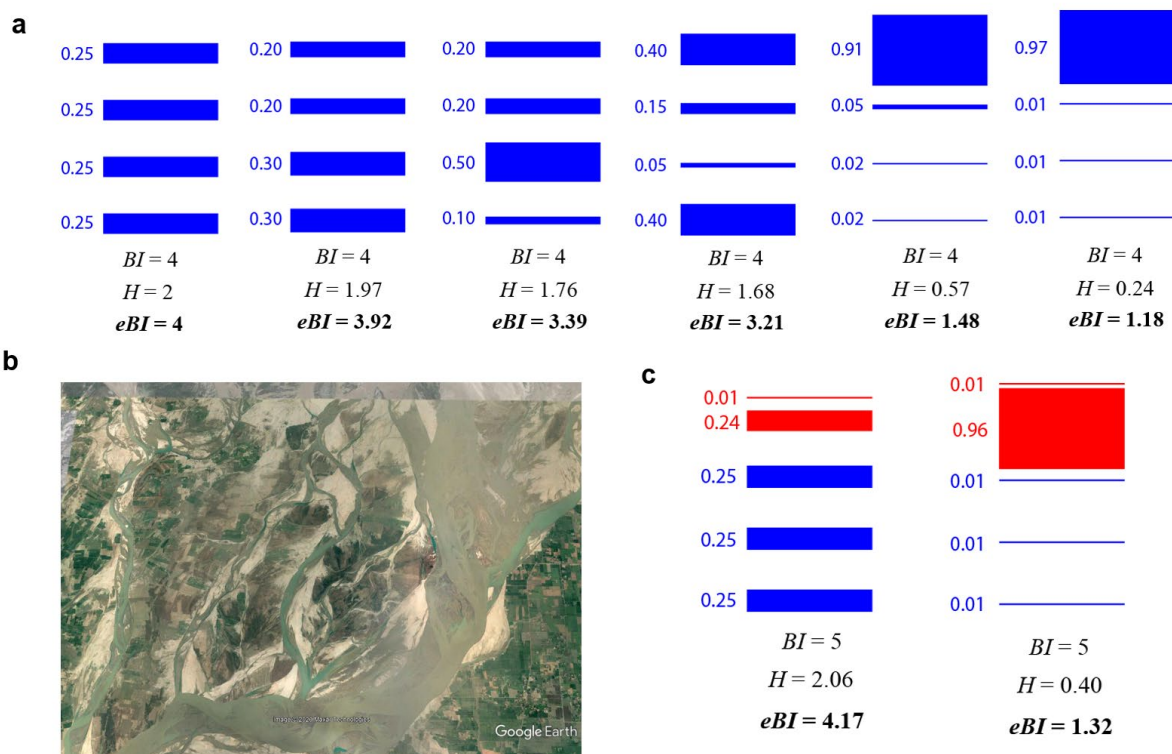
432

433

434

435

436 **Figures**



437

438 **Fig 1. Illustration of the difference between braiding index (BI) and entropic braiding index (eBI).** (a) *Channel*

439 *heterogeneity.* The illustration shows a schematic of 6 river cross-sections (columns), each containing 4 channels represented by

440 blue bands. The width of each band is considered here as a proxy for the relative discharge for each channel (indicated by the

441 number to the left of each band). While BI is 4 for all the six configurations, the values of Shannon entropy (H) decrease from left

442 (maximum value for 4 channels) to right. The eBI computed as 2^H is also displayed for each configuration. eBI can be interpreted

443 as the equivalent number of equally sized channels characterized by the same value of H . The value of eBI matches our intuition

444 as an integrative measure of the channel count while accounting the heterogeneity in channel scale. (b) *Field Example.* Section of

445 the Indus River illustrating the diversity of channels (in terms of width) which co-exist in river cross-sections. (c) *Effect of*

446 *resolution.* It displays two synthetic scenarios wherein we illustrate the change in BI and eBI when resolution is increased, and as

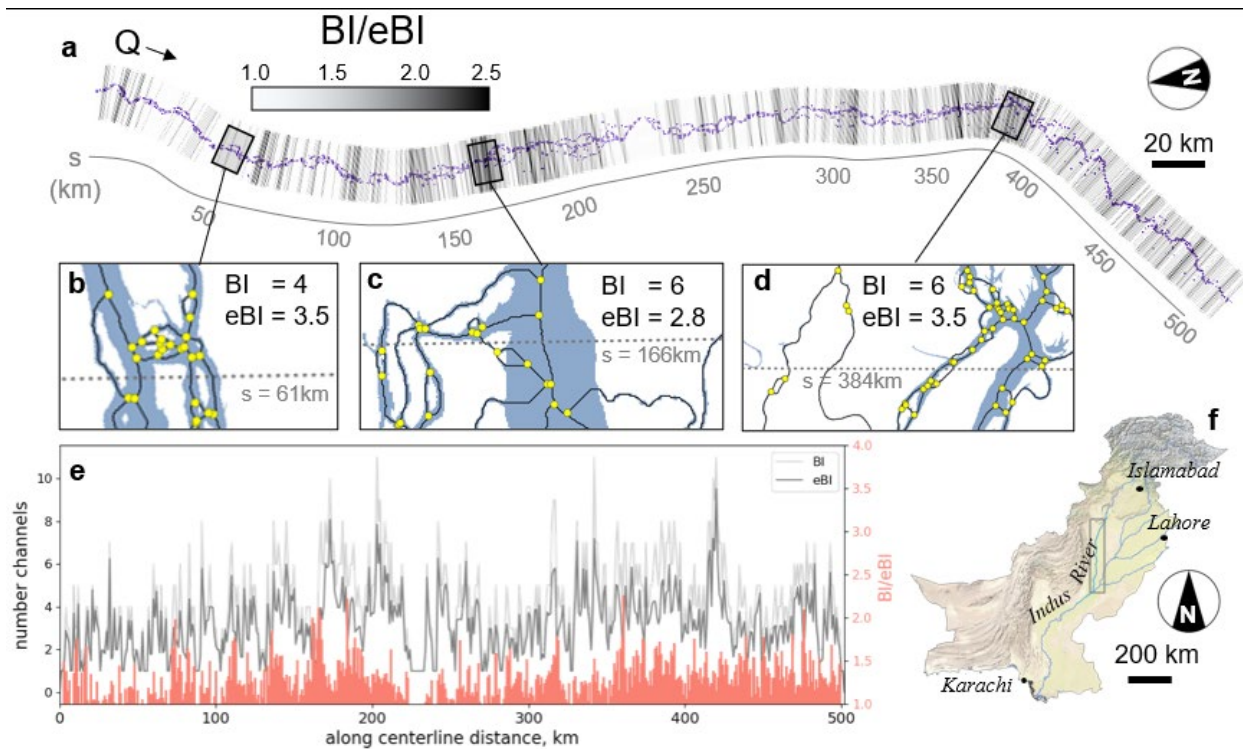
447 a result the number of channels visualized changes. Particularly the left (right) cross-section in (c) corresponds to the most left

448 (most right) cross-section from (a), where under an increased resolution scenario, the top channel (top blue band in a) is resolved

449 into two channels (to red bands in c). The new resolution scenario changes the value of BI from 4 to 5 for both configurations,

450 while eBI changes from 4 to 4.17 for the left cross-section and from 1.18 to 1.32 for the right cross-section, indicating a more

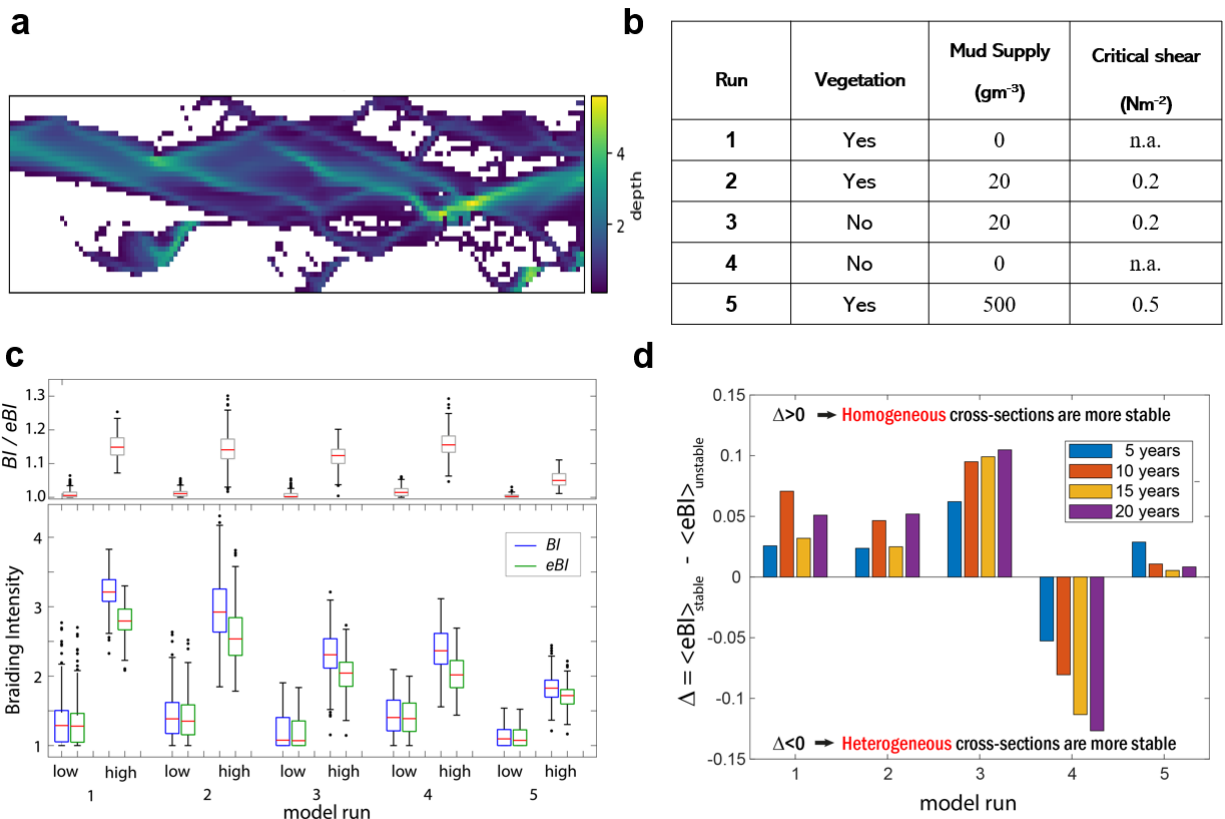
451 robust and relevant behavior of eBI in comparison with BI .



452

453 Fig 2. **Indus River.** (a) The Indus River (see panel f for reference) channel structure was extracted using RivGraph on the Global
 454 River Widths from Landsat product (Allen & Pavelsky, 2018). The cross-sections used for our analysis are marked with segments
 455 colored according to the value of the ratio BI/eBI . (b-c) Channel heterogeneity. Three different cross-sections are depicted in
 456 detail showing the channel network structure. These panels provide evidence of the variability in width of the co-existing
 457 channels per cross-section. (e) Braiding intensity. The values of BI (light gray), eBI (dark gray) are shown for each of the
 458 transects shown in a. The ratio BI/eBI is also displayed in pink, providing a quantitative measure of the diversity of channel
 459 widths along the river.

460



461

462

463

464

465

466

467

468

469

470

471

472

Fig 3. Numerically simulated multi-threaded channel. (a) *Model output.* Illustration of model output in terms of water depth field. (b) *Model runs.* Table containing the key parameters of the different model runs selected from Kleinhans et al., 2018. (c) *Braiding Intensity.* Comparison of the range of the values of *BI* (blue) *eBI* (green) and *BI/eBI* for each model run and for low and high levels of discharge. For each box plot, the lower and upper limit of the box represent the first (Q_1) and third (Q_3) quartiles respectively, while the horizontal line within the box (red) corresponds to the median. The whiskers extent 1.5 times the interquartile range (Q_3-Q_1) capped to the maximum/minimum value of the dataset. (d) *Cross-section stability.* Δ , i.e., mean difference of *eBI* for k -year 2-channel stable and k -year 2-channel unstable cross-sections ($k=5, 10, 15$ and 20 years) for each model run. Positive (negative) values of Δ indicate that stable (unstable) cross-sections exhibit more homogeneous cross-sections in terms of channel widths than unstable (stable) cross-sections, and therefore a larger number of effective channels. Our analysis shows that stable cross-sections consist of more homogeneous channels in the presence of vegetation and/or cohesive sediment, while channel disparity characterizes stable cross-sections for the run that have a sandy sediment supply and lack vegetation.